NASA TECHNICAL MEMORANDUM

NASA TM X-64519

THE POTENTIAL TEMPERATURE PROFILE IN THE PLANETARY BOUNDARY LAYER

By George H. Fichtl and Julian F. Nelson
Aero-Astrodynamics Laboratory

April 27, 1970

NASA

George C. Marshall Space Flight Center
Marshall Space Flight Center, Alabama

TECHNICAL REPORT STANDARD TITLE PAGE

1. REPORT NO. TM X-64519	2. GOVERNMENT ACCESSION NO.	3. RECIPIENT'S CATALOG NO.
4. TITLE AND SUBTITLE THE POTENTIAL TEMPERATURE PROFILE IN THE PLANETARY BOUNDARY LAYER		5. REPORT DATE April 27, 1970 6. PERFORMING ORGANIZATION CODE
7. AUTHOR(S) George H. Fichtl and Julian F. Nelson		8. PERFORMING ORGANIZATION REPORT #
9. PERFORMING ORGANIZATION NAME AND ADDRESS Aero-Astrodynamics Laboratory George C. Marshall Space Flight Center Marshall Space Flight Center, Alabama 35812		10. WORK UNIT NO. 11. CONTRACT OR GRANT NO. 13. TYPE OF REPORT & PERIOD COVERED Technical Memorandum
12. SPONSORING AGENCY NAME AND ADDRESS		14. SPONSORING AGENCY CODE

15. SUPPLEMENTARY NOTES

16. ABSTRACT

Nineteen observations of the temperature profile are used to analyze and to develop a model of the potential temperature profile $\bar{\theta}(z)$ in the planetary boundary layer. The observations consist of mean flow temperatures observed at the 3-, 18-, 30-, 60-, 120-, and 150-meter levels at the NASA meteorological tower site at Kennedy Space Center, Florida. It is provisionally concluded that the dimensionless potential temperature gradient $\phi_\theta = (z/T_{*o})\partial\bar{\theta}/\partial z$ is a function of z/L_o and $R_L = -fL_o/u_{*o}$, where T_{*o} and u_{*o} denote surface values of the friction temperature and friction velocity, L_o is the surface Monin-Obukhov stability length, and f is the Coriolis parameter. The expression $\phi_\theta = (1 - \gamma z/L_o)^{-1/2}$ summarizes the experimental results reasonably well, where γ is proportional to $R_L^{-3/2}$. The function ϕ_θ is integrated to yield the potential temperature profile and estimates of the potential temperature drop across the planetary boundary layer.

17. KEY WORDS	18. DISTRIBUTION STATEMENT FOR PUBLIC RELEASE: E. D. Geissler Director, Aero-Astrodynamics Laboratory

19. SECURITY CLASSIF. (of this report) UNCLASSIFIED	20. SECURITY CLASSIF. (of this page) UNCLASSIFIED	21. NO. OF PAGES 40	22. PRICE

MSFC - Form 3292 (May 1969)

ACKNOWLEDGEMENTS

The authors express their thanks to Mrs. Ella Mae McAllister of the Marshall Computation Laboratory who performed the programming and computations. In addition, we wish to thank Mr. Douglas Mackiernan of the Aero-Astrodynamics Laboratory who helped prepare the report.

DEFINITION OF SYMBOLS

Symbol	Definition
C_p	specific heat at constant pressure
f	Coriolis parameter ($2\Omega \sin \emptyset$)
g	acceleration of gravity
H_o	surface heat flux
k_1	von Karman's constant
K_H	eddy heat conduction coefficient
K_M	eddy viscosity coefficient
L_o	surface Monin-Obukhov length
$\bar{p}$	mean flow pressure
p_1	1,000 mb
R	specific gas constant for dry air
R_L	$-fL_o/u_{*o}$
Ri	gradient Richardson number
Ro	u_{*o}/fz_o, drag Rossby number
$\bar{T}$	mean flow Kelvin temperature
T_{*o}	surface friction temperature
$\bar{u}$	mean flow wind speed
u_{*o}	surface friction velocity
z	height above natural grade
z_o	surface roughness length

DEFINITION OF SYMBOLS (Continued)

Symbol	Definition
γ	a function of R_L
$\delta\bar{\theta}$	potential temperature drop across the planetary boundary layer
λ	$-\gamma z_o/L_o$, potential temperature profile parameter
$\bar{\theta}$	mean flow potential temperature
$\bar{\rho}$	mean flow density
τ_o	surface tangential stress
ϕ	latitude of observation site
ϕ_u	dimensionless wind shear
ϕ_θ	dimensionless potential temperature gradient
ψ	Monin layer wind profile stability defect, a universal function of z/L_o
Ω	angular velocity of earth

TECHNICAL MEMORANDUM X-64519

THE POTENTIAL TEMPERATURE PROFILE IN THE PLANETARY BOUNDARY LAYER

SUMMARY

The profile of mean flow potential temperature in the first 150 meters of unstable planetary boundary layer is analyzed with a sample of nineteen temperature profiles observed at the NASA 150-meter meteorological tower site. The observations consist of mean temperatures observed at 3-, 18-, 30-, 60-, 120-, and 150-meter levels. The duration time of each test ranged between approximately fifteen minutes to one hour.

It is hypothesized that the dimensionless potential temperature gradient $\phi_\theta = zT_{*o}^{-1}\partial\bar{\theta}/\partial z$ is a dimensionless function of z, L_o, f, and u_{*o}, where $\bar{\theta}(z)$ is the mean flow potential temperature at height z, T_{*o} and u_{*o} denote the surface values of the friction temperature and friction velocity, L_o is the surface Monin-Obukhov stability length, and f is the Coriolis parameter. According to Buckingham's theorem, only two independent dimensionless quantities can be constructed from the set z, L_o, f and u_{*o}; however, these dimensionless quantities can be chosen in a variety of ways. Accordingly, the dependencies of ϕ_θ on $(z/L_o, R_L)$-, $(z/L_o, fz/u_{*o})$-, and $(fz/u_{*o}, R_L)$-coordinates are examined, where $R_L = -fL_o/u_{*o}$. The function $\phi_\theta(z/L_o, R_L) = (1-\gamma z/L_o)^{-1/2}$ summarized the data reasonably well, where γ is a positive quantity proportional to $R_L^{-3/2}$ over the range of variation of the data. The functions $\phi_\theta(z/L_o, fz/u_{*o})$ and $\phi_\theta(fz/u_{*o}, R_L)$, derived from the function $\phi_\theta(z/L_o, R_L)$, agree with the experimental results.

Integration of the differential equation $\phi_\theta = \phi_\theta(z/L_o, R_L)$ yields the potential temperature profile. For sufficiently small values of the quantity $\lambda = -\gamma z_o/L_o$, the potential temperature profile has a logarithmic behavior with a linear defect resulting from stability and Coriolis effects, where z_o is the surface roughness length of the site. The potential temperature profile is used to evaluate the drop in potential temperature across the planetary boundary layer. The depth of the boundary layer is assumed to be $u_{*o}/4f$.

I. INTRODUCTION

This report concerns the vertical profile of mean flow potential temperature in the planetary boundary layer. In approximately the first 30 meters of the horizontally homogeneous planetary boundary layer, the Monin layer, the experimental results of Dyer [1], Pandolfo [2], and Prasad and Panofsky [3] imply that the potential temperature profile can be expressed functionally in the form

$$\bar{\theta} = F(z/L_o,\ z_o/L_o), \tag{1}$$

where z, L_o, and z_o denote the height, surface Monin-Obukhov stability length, and the surface roughness length. The mean flow wind profile is also a function of z/L_o and z_o/L_o in the Monin layer. However, as we proceed upward out of the Monin layer into the Ekman layer, we find that the Coriolis forces must be taken into account in order to explain the behavior of the wind profile [4, 5]. In view of the inherent coupling between the vertical turbulent momentum and heat fluxes and the mean flow wind and potential temperature profiles implied by the mean-flow Boussinesq-approximated equations of motion [6], it is reasonable to expect that the potential temperature profile is also affected by the Coriolis terms in the momentum conservation equations. The data analysis that follows shows that this appears to be the case.

II. DIMENSIONAL CONSIDERATIONS

In the Monin layer the vertical gradient of mean flow potential temperature $\partial\bar{\theta}/\partial z$ is scaled with the height z and the surface friction temperature T_{*o}. The resulting dimensionless temperature gradient is a universal function of z/L_o, so that

$$\frac{z}{T_{*o}}\frac{\partial\theta}{\partial z} = \phi_\theta(z/L_o). \tag{2}$$

The quantity L_o is the surface Monin-Obukhov stability length and is given by

$$L_o = -\frac{C_p\bar{\rho}\ \bar{T}\ u_{*o}^3}{k_1 g\ H_o}\ , \tag{3}$$

where u_{*o} is the surface friction velocity, k_1 is von Karman's constant with a numerical value approximately equal to 0.4, $\bar{T}$ and $\bar{\rho}$ denote the mean temperature and density in the boundary layer, g is the acceleration of gravity, and H_o is the surface heat flux. The surface friction temperature is defined as

$$T_{*o} = - \frac{H_o}{k_1 u_{*o} \bar{\rho}\, C_p} \ . \tag{4}$$

Integration of equation (2) from z_o to z, subject to the boundary condition that

$$\bar{\theta} = \bar{\theta}(z_o/L_o) \quad \text{at} \quad z/L_o = z_o/L_o, \tag{5}$$

will yield the potential temperature profile

$$\bar{\theta}(z/L_o) = \bar{\theta}(z_o/L_o) + T_{*o} \left\{ \ln \frac{z}{z_o} - \int_{-z_o/L_o}^{-z/L_o} \frac{1 - \phi_\theta(x)}{x}\, dx \right\} . \tag{6}$$

Note that the surface roughness length appears in the potential temperature profile through the boundary condition (5).

In the Ekman layer, ϕ_θ should also be a function of z and L_o and other parameters that characterize the action of Coriolis forces, baroclinic effects, etc. In this report, we are concerned with determining the effects of the vertical heat and momentum fluxes and the Coriolis forces on the potential temperature profile. The parameter L_o should be sufficient to characterize the effects resulting from the turbulent momentum and heat fluxes. To represent the effects of Coriolis forces, we could add the Coriolis parameter f to our list of independent variables.* Thus, we might suspect that ϕ_θ should depend on z, L_o, and f; however, it is not possible to construct a dimensionless quantity that contains f with this list of independent variables, because z and L_o have the units of length and f is an inverse time.

*The Coriolis parameter is defined as $f = 2\Omega \sin \phi$, where Ω is the angular velocity of the earth and ϕ denotes the latitude of the site.

Thus, at least one additional parameter must be included in the dimensional analysis. Blackadar and Tennekes [4] have shown that u_{*o} is the appropriate velocity scale in the planetary boundary layer by analyzing the turbulent energy equation. The addition of u_{*o} to our list of pertinent parameters will enable us to construct a dimensionless quantity which will contain f. This follows from the fact that u_{*o}/f has the units of length. In fact, an estimate of the thickness of the planetary boundary layer is $u_{*o}/4f$ [4], so that the addition of u_{*o} to our list of independent variables is physically relevant. As in the case of the Monin layer, we will not include z_o in the list of variables upon which we hypothesize ϕ_θ to depend. However, z_o will enter the analysis through the boundary condition, equation (5), when we integrate ϕ_θ to obtain the potential temperature profile.

According to Buckingham's theorem [7], the number of a complete set of independent dimensionless quantities that can be constructed from the set of four variables z, L_o, f, and u_{*o} is two. There are many possible ways to construct these dimensionless quantities. Three possible representations are given by

$$\left.\begin{array}{lll} \text{Set I:} & \dfrac{z}{L_o}, & \dfrac{fL_o}{u_{*o}} \\[2ex] \text{Set II:} & \dfrac{z}{L_o}, & \dfrac{fz}{u_{*o}} \\[2ex] \text{Set III:} & \dfrac{fz}{u_{*o}}, & \dfrac{fL_o}{u_{*o}} \end{array}\right\} . \qquad (7)$$

These dimensionless quantities are the simplest representations since they are constructed from the independent variables raised only to the first power. All other formulations would require lower or higher order exponents. Any one set of the dimensionless quantities given by (7) can be derived from any one of the remaining two sets by forming appropriate ratios. Each set has its own merits so that, rather than selecting one formulation of the problem, we will examine the following three representations of ϕ_θ:

$$\phi_\theta = \phi_\theta(z/L_o, R_L) \qquad (8)$$

$$\phi_\theta = \phi_\theta(z/L_o,\ fz/u_{*o}) \tag{9}$$

$$\phi_\theta = \phi_\theta(fz/u_{*o},\ R_L), \tag{10}$$

where

$$R_L = -\frac{fL_o}{u_{*o}} . \tag{11}$$

III. THE DATA SOURCE AND DATA PROCESSING

The data analyzed in this report consist of nineteen sets of temperature measurements at the 3-, 18-, 30-, 60-, 120-, and 150-meter levels and associated wind speed measurements at the 18- and 30-meter levels obtained at NASA's 150-meter meteorological tower site. The instrumentation of this tower site has been discussed by Kaufman and Keene [8]. The azimuthal distribution of the surface roughness z_o at the KSC tower site is discussed in reference 9, and the temporal mean temperature and wind data are tabulated in Appendix B. The duration of each case ranged between approximately fifteen minutes to one hour; however, the majority of cases had a duration time of one hour. The calculation of u_{*o}, T_{*o}, and L_o for each case is discussed in Appendix A, and the results of the calculations are tabulated in Appendix B.

The mean flow potential temperature $\bar{\theta}$, Kelvin temperature $\bar{T}$, and pressure $\bar{p}$ are related through Poisson's equation

$$\bar{\theta} = \bar{T}(p_1/\bar{p})^{R/C_p} , \tag{12}$$

where p_1 = 1,000 mb and R is the specific gas constant for dry air. Partial differentiation of this equation with respect to z yields the result

$$\frac{\partial\bar{\theta}}{\partial z} = \frac{\bar{\theta}}{\bar{T}}\left(\frac{\partial\bar{T}}{\partial z} + \frac{g}{C_p}\right) . \tag{13}$$

Equation (13) was used to obtain a first estimate of $\partial\bar{\theta}/\partial z$, with the assumption that $\bar{\theta}/\bar{T} \simeq 1$. The derivative $\partial\bar{T}/\partial z$ was estimated at the mid-points between the data acquisition levels with finite central differences. The resulting estimates of $\partial\bar{\theta}/\partial z$ were multiplied by correction factors to account for the errors resulting from the finite difference operators. These corrections were based on the assumption that $\partial\bar{\theta}/\partial z \propto z^q$ over piecewise portions of the potential temperature profile, where q is a constant. The details of this correction and its application are discussed in Appendix C.

IV. DIMENSIONLESS POTENTIAL TEMPERATURE GRADIENTS

The ranges of the experimental values of R_L and fz/u_{*o} were $0.0004 < R_L < 0.05$ and $0.0007 < fz/u_{*o} < 0.03$. The nineteen potential temperature profiles were grouped according to the categories of R_L given in Table I and the ninety-five estimates of the dimensionless potential temperature gradient were grouped according to the categories of fz/u_{*o} given in Table II. Figures 1 through 3 are plots of the experimental values of $\phi_\theta(z/L_o, R_L)$, $\phi_\theta(z/L_o, fz/u_{*o})$, and $\phi_\theta(fz/u_{*o}, R_L)$ with the data points grouped according to the categories in Tables I or II.

TABLE I

Potential Temperature Profile Categories According to R_L

Category	No. of Profiles
$0.0004 < R_L < 0.0007$	2
$0.001 < R_L < 0.003$	4
$0.005 < R_L < 0.01$	5
$0.01 < R_L < 0.03$	6
$0.04 < R_L < 0.05$	2

TABLE II

Potential Temperature Profile Categories According to fz/u_{*o}

	No. of Observations
$0.0007 < fz/u_{*o} < 0.001$	4
$0.001 < fz/u_{*o} < 0.002$	16
$0.002 < fz/u_{*o} < 0.004$	17
$0.004 < fz/u_{*o} < 0.006$	14
$0.006 < fz/u_{*o} < 0.01$	15
$0.01 < fz/u_{*o} < 0.03$	29

Figure 1 shows that $\emptyset_\theta$ is an increasing function of z/L_o for fixed R_L and an increasing function of R_L for fixed z/L_o. It might be concluded from these results that the presence of Coriolis forces tends to promote stability in the sense that an increase in f will tend to produce an increase in $\partial\bar{\theta}/\partial z$, all other things being equal.

Figure 2 shows that $\emptyset_\theta$ is an increasing function of z/L_o for fixed fz/u_{*o} and an increasing function of fz/u_{*o} for fixed z/L_o. Figure 3 implies that $\emptyset_\theta$ is a decreasing function of fz/u_{*o} for fixed R_L and an increasing function of R_L for fixed fz/u_{*o}. The upper bound value on $\emptyset_\theta$ is of order one, while the lower bound appears to approach zero like $(z/L_o)^{-1/2}$ for fixed R_L in figure 1, $(z/L_o)^{-5/4}$ for fixed fz/u_{*o} in figure 2, and $(fz/u_{*o})^{-1/2}$ for fixed R_L in figure 3.

The Businger hypothesis states that in the Monin layer the flux Richardson number

$$Ri = \frac{\frac{g}{\bar{\theta}}\frac{\partial\bar{\theta}}{\partial z}}{(\partial\bar{u}/\partial z)^2} \tag{14}$$

is related to L_o through the expression

$$Ri = z/L_o, \tag{15}$$

where $\bar{u}$ is the mean wind at height z. Experimental investigations [6] imply that the dimensionless wind shear $\emptyset_u = (k_1 z/u_{*o})\partial\bar{u}/\partial z$ in the Monin layer is given by

$$\emptyset_u = (1 - 18Ri)^{-1/4}. \tag{16}$$

Upon combining (3), (4), (14), (15), and (16), we find that

$$\emptyset_\theta = (1 - 18z/L_o)^{-1/2}. \tag{17}$$

Thus, as $-z/L_o$ becomes large in the unstable Monin layer, $\emptyset_\theta$ asymptotically behaves like

$$\emptyset_\theta \sim 18^{-1/2}(z/L_o)^{-1/2}. \tag{18}$$

We should be able to obtain this asymptotic behavior from our data as $R_L \rightarrow 0$. The experimental values of ϕ_θ in Figure 2 tend to decrease as $(-z/L_o)^{-1/2}$ as $-z/L_o$ becomes large for the smaller values of R_L. However, the coefficient of $(-z/L_o)^{-1/2}$ in equation (18) is not obtained as R_L becomes small, but rather the data appear to imply that the coefficient increases to values greater than $18^{-1/2}$ as R_L becomes small. This will become more obvious below.

To develop a model of ϕ_θ for the planetary boundary layer, it is assumed that

$$\phi_\theta(z/L_o, R_L) = (1 - \gamma z/L_o)^{-1/2}, \tag{19}$$

where γ is now a function of R_L. When $\gamma = 18$, we obtain equation (17). The function γ was determined by fitting equation (19) to each potential temperature profile with least-square procedures. The results of these computations are shown in Figure 4. Three of the profiles yielded negative values of γ which were approximately equal to zero for $R_L = 0.0237$, 0.0415, and 0.0474. However, these data points fit in with the overall trend implied by the data points in Figure 4, namely, γ being a decreasing function of R_L. A least-squares analysis of the sixteen data points in Figure 4 yielded the result

$$\gamma = 0.0044\ R_L^{-3/2}. \tag{20}$$

It is of interest to note that the geometric mean value of γ is equal to 16, which is not significantly different from the value of 18 in equation (17).

Dyer [1] has analyzed experimental estimates of ϕ_θ in the Monin layer and finds that

$$\phi_\theta = (1 - 15z/L_o)^{-0.55}. \tag{21}$$

This result is not significantly different from equation (17). Prasad and Panofsky [3] find that equation (17) summarizes the temperature observations in their analysis. However, the largest value of $-z/L_o$ in these studies was on the order of one. It can be seen from the results in Figure 1 that it would be rather difficult to find a dependence of γ on R_L if we restricted the analysis to the data points associated with $-z/L_o < 1.0$. The large values of $-z/L_o$ in this study were primarily obtained by making temperature measurements at sufficiently great heights (150 meter tower). Dyer [1] obtained his temperature measurements at various height intervals up to a maximum height of 16 m. The temperature data used by Prasad and Panofsky [3] were obtained from various tower sites at heights between the 1- and 46-meter levels. In view of the result given by equation (20), we tentatively conclude that the result given by equation (17) for the Monin layer is not an asymptotic result as R_L approaches zero, but rather, equation (17) yields values of ϕ_θ associated with typical values of $R_L \simeq 0.004$.

Figure 8 is a plot of the experimental values of ϕ_θ as a function of $\gamma z/L_o$, where γ is calculated with equation (20). The function given by (19) is a good fit to the data, and a comparison of Figures 1 and 8 shows that the experimental scatter is reduced significantly by permitting the quantity γ to be a function of R_L.

Upon combining equations (19) and (20), we find that

$$\phi_\theta(z/L_o, R_L) = (1 - 0.0044 R_L^{-3/2}\, z/L_o)^{-1/2}. \tag{22}$$

A plot of ϕ_θ as a function of z/L_o for various values of R_L, according to equation (22), is shown in Figure 5. For sufficiently large $-z/L_o$ or small R_L, we have the asymptotic behavior

$$\phi_\theta(z/L_o, R_L) \sim (0.0044)^{-1/2}\, R_L^{3/4}(-z/L_o)^{-1/2}. \tag{23}$$

A comparison of Figures 1 and 5 will show that the expression given by (22) is a reasonably good fit to the data.

Equation (22) can be cast into two alternate forms, namely,

$$\phi_\theta(z/L_o, fz/u_{*o}) = (1 + 0.0044(fz/u_{*o})^{-3/2}(-z/L_o)^{5/2})^{-1/2} \tag{24}$$

and

$$\phi_\theta(fz/u_{*o}, R_L) = (1 + 0.0044\, R_L^{-5/2}\, fz/u_{*o})^{-1/2}. \tag{25}$$

These functions are given in Figures 6 and 7. For sufficiently large $-z/L_o$ or small fz/u_{*o}, we obtain from (24) the result

$$\phi_\theta(z/L_o, fz/u_{*o}) \sim (0.0044)^{-1/2} (fz/u_{*o})^{3/4} (-z/L_o)^{-5/4}, \qquad (26)$$

while for sufficiently large fz/u_{*o} or small R_L, we obtain from (25)

$$\phi_\theta(fz/u_{*o}, R_L) \sim (0.0044)^{-1/2} R_L^{5/4} (fz/u_{*o})^{-1/2}. \qquad (27)$$

These results are consistent with the experimental results in Figures 2 and 3.

V. POTENTIAL TEMPERATURE PROFILE

Integration of the differential equation (19), subject to the boundary condition (5), will yield the potential temperature profile for any particular value of R_L, so that

$$\frac{\Delta\theta(z/z_o)}{T_{*o}} = \ln\left\{\frac{(1 + \lambda z/z_o)^{1/2} - 1}{(1 + \lambda z/z_o)^{1/2} + 1} \cdot \frac{(1 + \lambda)^{1/2} + 1}{(1 + \lambda)^{1/2} - 1}\right\}, \qquad (28)$$

where

$$\lambda = -\gamma z_o/L_o \qquad (29)$$

$$\Delta\bar{\theta}(z/z_o) = \bar{\theta}(z/z_o) - \bar{\theta}(1). \qquad (30)$$

Figure 9 depicts $\Delta\bar{\theta}(z/z_o)/T_{*o}$ as a function of z/z_o for various values of λ. As $R_L \to \infty$, the quantity $\lambda \to 0$ and the function (29) has the asymptotic behavior

$$\frac{\Delta\theta(z/z_o)}{T_{*o}} \sim \ln\frac{z}{z_o} - 0.0011 R_L^{-5/2} Ro^{-1}(\frac{z}{z_o} - 1), \qquad (31)$$

where Ro is the drag Rossby number given by

$$Ro = u_{*o}/fz_o. \tag{32}$$

Thus, for sufficiently large R_L, we have a logarithmic potential temperature profile with a linear defect.

An estimate of the potential temperature drop $\delta\bar{\theta}$ across the planetary boundary can be obtained by evaluating equation (28) at the top of the boundary layer $z = u_*/4f$, so that

$$\frac{\delta\bar{\theta}}{T_{*o}} = \ln\left\{\frac{(1 + \gamma/4R_L)^{1/2} - 1}{(1 + \gamma/4R_L)^{1/2} + 1} \cdot \frac{(1 - \gamma z_o/L_o)^{1/2} + 1}{(1 - \gamma z_o/L_o)^{1/2} - 1}\right\}. \tag{33}$$

We can also express this result in the form

$$\frac{\delta\bar{\theta}}{T_{*o}} = \ln\left\{\frac{(1 + \gamma/4R_L)^{1/2} - 1}{(1 + \gamma/4R_L)^{1/2} + 1} \cdot \frac{(1 + \gamma/R_L Ro)^{1/2} + 1}{(1 + \gamma/R_L Ro)^{1/2} - 1}\right\}. \tag{34}$$

As R_L approaches zero, the quantity γ approaches zero, so that upon expanding (34) in series, we find that

$$\frac{\delta\bar{\theta}}{T_{*o}} \sim \ln\frac{Ro}{4} - 0.0022\, R_L^{-5/3}\left(\frac{1}{4} - Ro^{-1}\right) + \ldots\ . \tag{35}$$

This result shows that for sufficiently near neutral atmospheres, or atmospheres with sufficiently large rotation rates (f), the dimensionless potential temperature drop across the planetary layer is asymptotically equal to $\ln(Ro/4)$ as R_L approaches infinity.

As z_o/L_o becomes small, equation (33) behaves like

$$\frac{\delta\bar{\theta}}{T_{*o}} \sim -\ln\left(-\frac{\gamma}{4}\frac{z_o}{L_o}\right) + \ln\left\{\frac{(1 + \gamma/4R_L)^{1/2} - 1}{(1 + \gamma/4R_L)^{1/2} + 1}\right\}. \tag{36}$$

For sufficiently small R_L, the second term on the right-hand side of (36) is negligibly small, so that

$$\frac{\delta\bar{\theta}}{T_{*o}} \sim \ln(227.3R_L^{5/2}Ro). \qquad (37)$$

This corresponds to the case in which the boundary layer is very unstable. If we would have neglected Coriolis effects <u>ab initio</u> and set $\gamma = 18$, then the result that corresponds to (37) is

$$\frac{\delta\bar{\theta}}{T_{*o}} \sim -\ln(-4.5z_o/L_o), \qquad (38)$$

or in terms of R_L and Ro,

$$\frac{\delta\bar{\theta}}{T_{*o}} \sim \ln(0.222R_L Ro). \qquad (39)$$

VI. SECOND- AND THIRD-ORDER CONSIDERATIONS

To facilitate the discussion that follows, let us denote ϕ_u and ϕ_θ as given by (16) and (17) with $\phi_u^{(1)}$ and $\phi_\theta^{(1)}$ and the associated value of $\gamma(=18)$ with $\gamma^{(1)}$. The calculations of the scaling temperature T_{*o} and scaling velocity u_{*o} were based on $\phi_u^{(1)}$ (see Appendix A). However, the experimental estimates of ϕ_θ in Figure 1, $\phi_\theta^{(2)}$ say, implied that γ is not a constant equal to 18, but rather that γ is a function of R_L, and we will denote this function with $\gamma^{(2)}$. Thus, in a manner of speaking, we have deduced the second-order function $\phi_\theta^{(2)}$ with the aid of the first-order Monin layer through $\phi_u^{(1)}$. According to Businger's hypothesis, $\phi_u = \phi_\theta^{1/2}$ in the Monin layer; therefore, we might infer that in the Monin layer the second-order dependence of ϕ_u on R_L resulting from the second-order potential temperature profile is

$$\phi_u^{(2)} = (1 - \gamma^{(2)}\, z/L_o)^{-1/4}. \qquad (40)$$

This result will be used to obtain new estimates of T_{*o} and u_{*o}, and thus third-order estimates of ϕ_θ and γ. Henceforth, a numerical parenthetical superscript will denote the order of the quantity in question.

To analyze the effects of the third-order corrections on γ, it is useful to write $\phi_u^{(2)}$ in the form

$$\phi_u^{(2)} = (1 - 18z/L_o^{(2)})^{-1/4}, \tag{41}$$

where

$$L_o^{(2)} = 18L_o/\gamma^{(2)}. \tag{42}$$

The wind profile that corresponds to (41) can be written in the form

$$\bar{u}^{(2)}(z) = \frac{u_{*o}^{(2)}}{k_1}\left\{\ln\frac{z}{z_o} - \psi^{(2)}\,(z/L_o^{(2)})\right\}, \tag{43}$$

where

$$\psi^{(2)}(z/L_o^{(2)}) = \int_o^{-z/L_o^{(2)}} \frac{1 - \phi_u^{(2)}(\xi)}{\xi}\,d\xi \tag{44}$$

and ξ is a variable of integration associated with $z/L_o^{(2)}$. The ratios between the first- and second-order scaling parameters are

$$\frac{u_{*o}^{(2)}}{u_{*o}^{(1)}} = \frac{\ln(z/z_o) - \psi^{(1)}(z/L_o^{(1)})}{\ln(z/z_o) - \psi^{(2)}(z/L_o^{(2)})} \tag{45}$$

$$\frac{T_{*o}^{(2)}}{T_{*o}^{(1)}} = \left\{\frac{\ln(z/z_o) - \psi^{(1)}(z/L_o^{(1)})}{\ln(z/z_o) - \psi^{(2)}(z/L_o^{(2)})}\right\}^2, \tag{46}$$

where $\psi^{(1)}(z/L_o^{(1)})$ is the first-order counterpart of $\psi^{(2)}(z/L_o^{(2)})$. The 18-meter level wind speed was used to obtain $u_{*o}^{(1)}$ and $T_{*o}^{(1)}$, so that $z = 18$ m and $z_o \simeq 0.2$ m at the NASA 150-meter tower site. If $\gamma^{(2)} = 18$, then $z/L_o^{(2)} = z/L_o$, and it follows from (45) and (46) that $u_{*o}^{(2)} = u_{*o}^{(1)}$ and $T_{*o}^{(2)} = T_{*o}^{(1)}$. If $\gamma^{(2)}$ is less than 18, then $-z/L_o^{(2)}$ is less than $-(z/L_o^{(1)})$, which implies $\psi^{(2)}(z/L_o^{(2)}) < \psi^{(1)}(z/L_o^{(1)})$, and we conclude from (45) and (46) that $u_{*o}^{(2)}$ is less than $u_{*o}^{(1)}$ and $|T_{*o}^{(2)}|$ is less than $|T_{*o}^{(1)}|$. If $\gamma^{(2)}$ is greater than 18, the inequalities are reversed so that $u_{*o}^{(2)}$ is greater than $u_{*o}^{(1)}$ and $|T_{*o}^{(2)}|$ is greater than $|T_{*o}^{(1)}|$. At $z/L_o = 0$, we have $u_{*o}^{(2)} = u_{*o}^{(1)}$ and $T_{*o}^{(2)} = T_{*o}^{(1)}$, and the ratios $u_{*o}^{(2)}/u_{*o}^{(1)}$ and $T_{*o}^{(2)}/T_{*o}^{(1)}$ depart from unity as $-z/L_o$ approaches infinity. Now $\phi_\theta^{(3)}$ is directly proportional to $T_{*o}^{(2)}$ and $R_L^{(3)}$ is inversely proportional to $u_{*o}^{(2)}$. This means that the third-order estimates of γ, $\gamma^{(3)}$, will lie below and to the right of their corresponding estimates of $\gamma^{(2)}$ for $\gamma^{(2)} < 18$ and above and to the left of their corresponding estimates of $\gamma^{(2)}$ for $\gamma^{(2)} > 18$. The third-order estimates of γ are shown in Figure 10. A least-squares fit to the data points in this figure yields the result

$$\gamma^{(3)} = 0.0012(R_L^{(2)})^{-7/4}.$$

This function is depicted in Figure 9 along with the functions $\gamma^{(1)}$ and $\gamma^{(2)}$. The results in the figure show that this correction procedure seems to converge. The differences between $\gamma^{(2)}$ and $\gamma^{(3)}$ are probably not significant because $\gamma^{(2)}$ lies well within the data scatter of $\gamma^{(3)}$ and vice versa.

The question that must now be answered is whether or not the function $\phi_u^{(2)}$ as expressed by (40) is physically real or just a spurious result. This can be answered only by analyzing wind and temperature profile measurements with corresponding direct measurements of the surface tangential stresses and heat fluxes.

VII. CONCLUDING COMMENTS

We have analyzed three representations of ϕ_θ in the planetary boundary layer, namely, $\phi_\theta(z/L_o,R_L)$, $\phi_\theta(z/L_o, fz/u_{*o})$, and $\phi_\theta(fz/u_{*o}, R_L)$. However, it is reasonable to expect that ϕ_θ should depend on other parameters. For example, it is well known that baroclinic effects manifested by the pressure gradient terms in the horizontal momentum conservation equations produce significant effects on the wind profile [11], and it is not unreasonable to assume that these effects are also reflected in the potential temperature profile. The available results of investigations of the wind profile in the planetary boundary layer could be used to suggest those additional parameters that should be included in future attempts to model the potential temperature profile.

In our analysis we developed an empirical model of $\phi_\theta(z/L_o,R_L)$, and from this function we deduced the functions $\phi_\theta(z/L_o, fz/u_{*o})$ and $\phi_\theta(fz/u_{*o},R_L)$ which agreed reasonably well with the experimental results. However, in studies of this kind, one must be careful to avoid or to at least recognize the problem of the spurious correlation which results when a scaling parameter occurs in two or more dimensionless quantities. In this report, the scaling temperature T_{*o} was derived from the estimates of L_o and u_{*o}, so that ϕ_θ is proportional to $zL_o u_{*o}^{-2}\, \partial\bar{\theta}/\partial z$. Thus, by the very fact that (1) z and L_o are contained in ϕ_θ and z/L_o, (2) u_{*o} and L_o are contained in ϕ_θ and R_L, and (3) z and u_{*o} are contained in ϕ_θ and fz/u_{*o}, the dependencies of ϕ_θ on $(z/L_o,R_L)$-, $(z/L_o,fz/u_{*o})$-, and $(fz/u_{*o},R_L)$-coordinates implied in Figures 1 through 3 could be spurious. This problem can be resolved by increasing the sample size and applying appropriate statistical significance tests.

To verify the results in this report, simultaneous observations of the potential temperature profile, the surface heat flux H_o, and the surface tangential stress τ_o are required. The measurements of the potential temperature profile should extend up to sufficiently great heights in the Ekman layer ($z \sim O(u_{*o}/4f)$). The problem of spurious correlation between ϕ_θ and the various independent variables will still remain, because T_{*o} is proportional to $H_o\tau_o^{-1/2}$ and L_o is proportional to $\tau_o^{3/2}H_o^{-1}$ so that ϕ_θ, z/L_o, R_L and fz/u_{*o} are proportional to

$$z\tau_o^{1/2}H_o^{-1}\partial\bar{\theta}/\partial z, \quad z\tau_o^{-3/2}H_o, \quad \tau_o H_o^{-1}, \quad \text{and} \quad z\tau_o^{-1/2},$$

respectively. The quantity τ_o is contained in all four of these quantities; H_o is present in ϕ_θ, z/L_o, and R_L; and the height z is contained in ϕ_θ, z/L_o, and fz/u_{*o}.

With these comments in mind, we provisionally conclude that the potential temperature profile in the planetary boundary layer is influenced by the action of Coriolis forces on the mean flow.

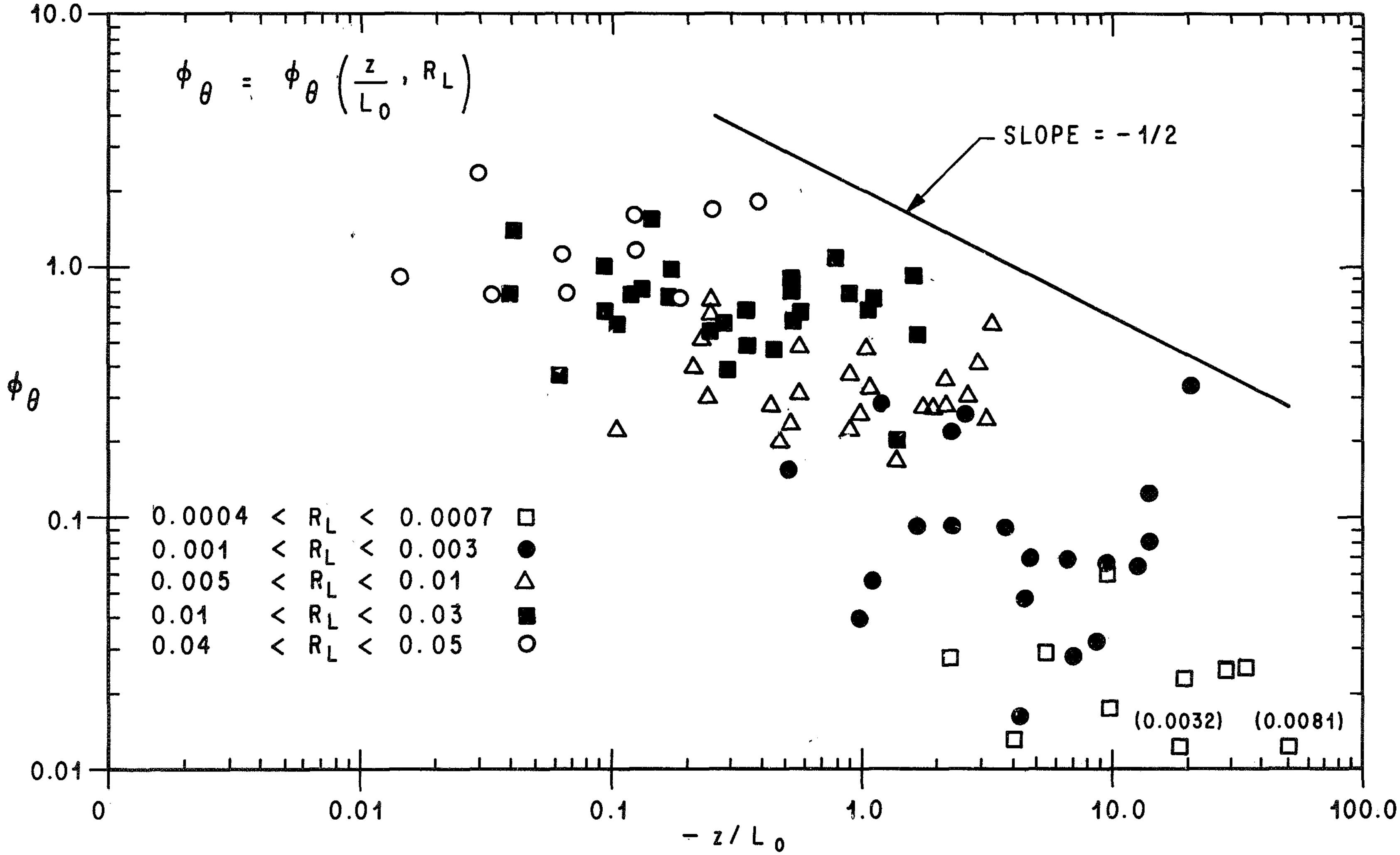

Figure 1. Experimental Values of ϕ_θ as a Function of z/L_o and R_L

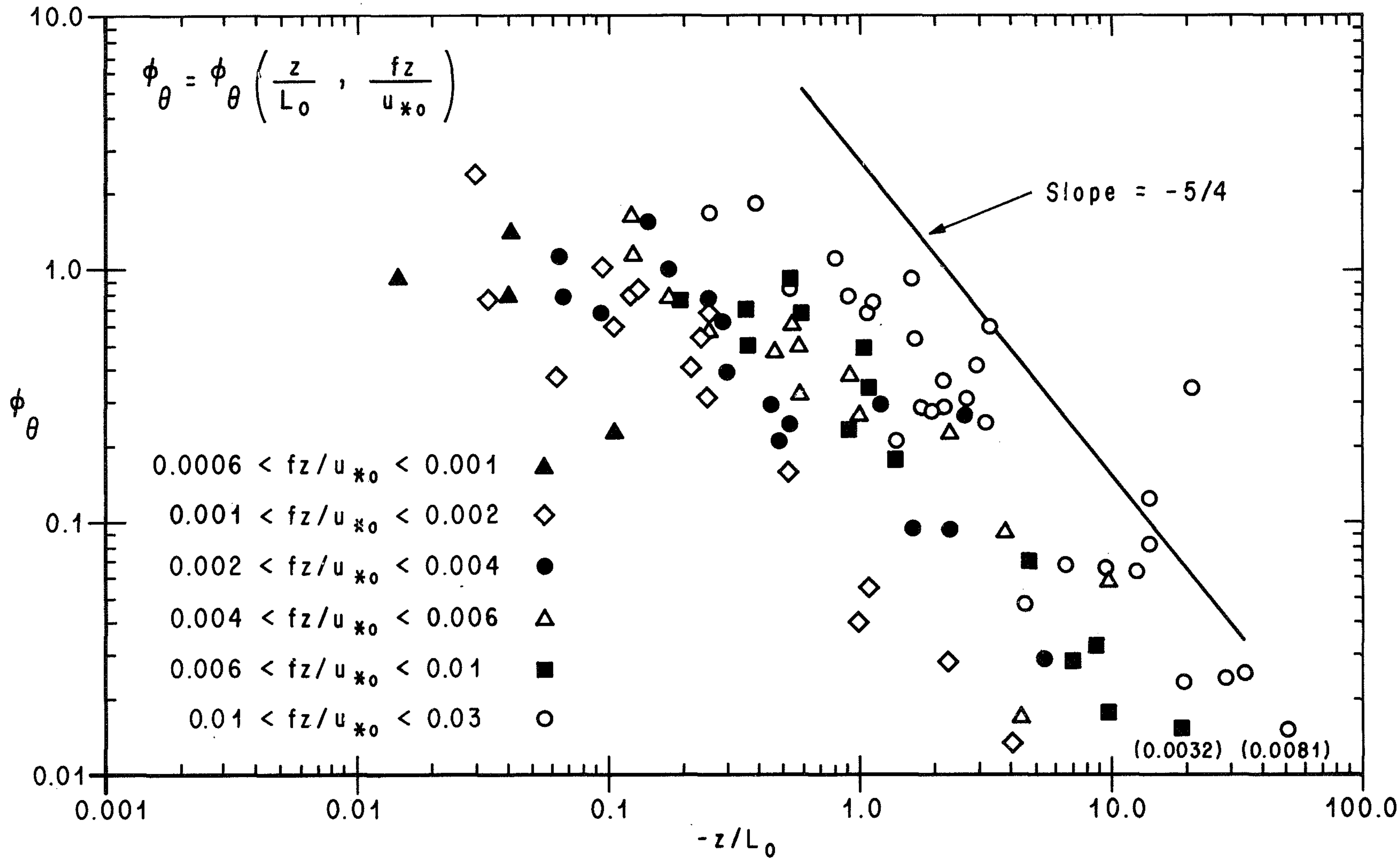

Figure 2. Experimental Values of ϕ_θ as a Function of z/L_o and fz/u_{*o}

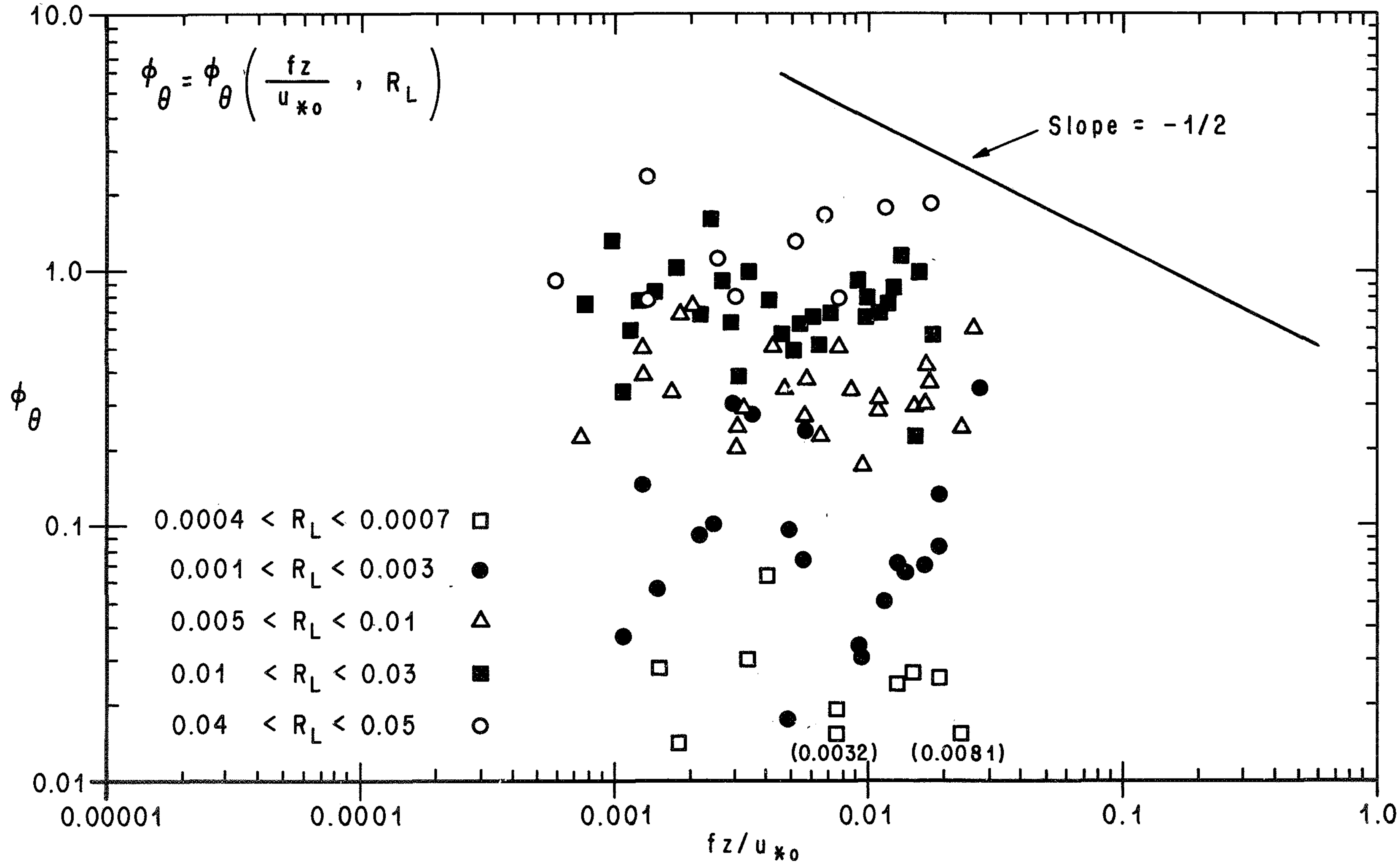

Figure 3. Experimental Values of ϕ_θ as a Function of fz/u_{*o} and R_L

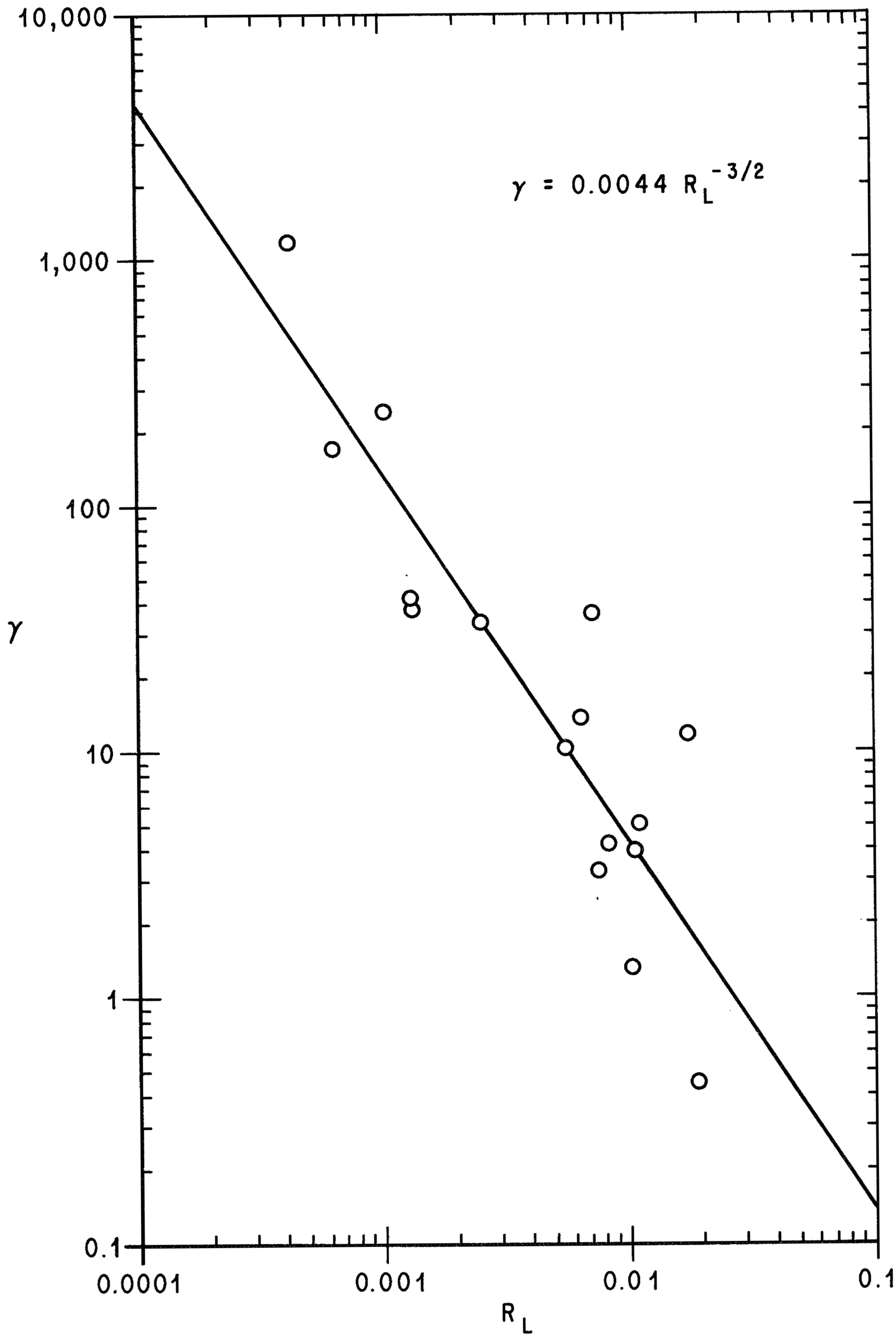

Figure 4. The Quantity γ as a Function of R_L

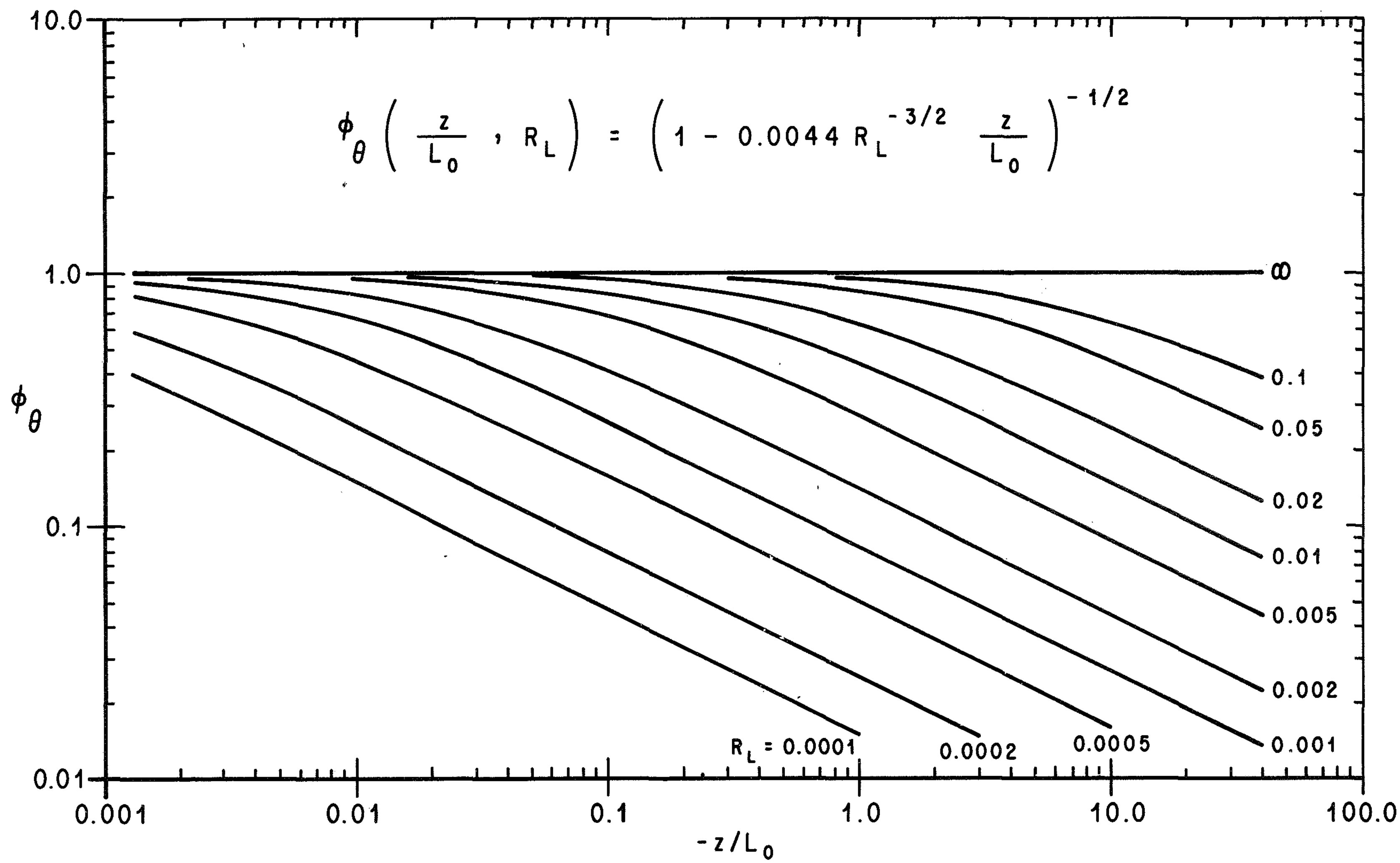

Figure 5. The Quantity ϕ_θ as a Function of z/L_0 and R_L

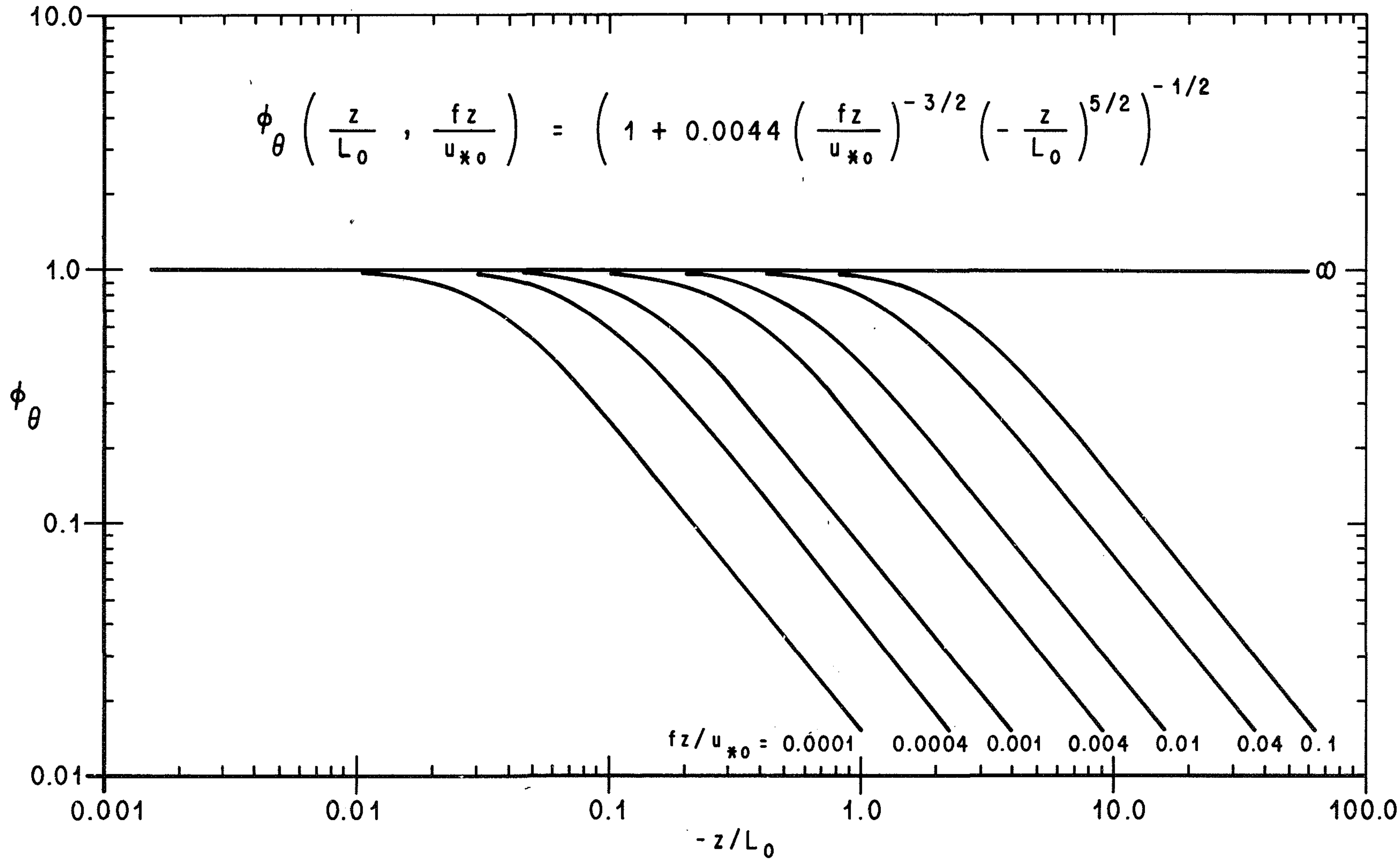

Figure 6. The Quantity ϕ_θ as a Function of z/L_o and fz/u_{*o}

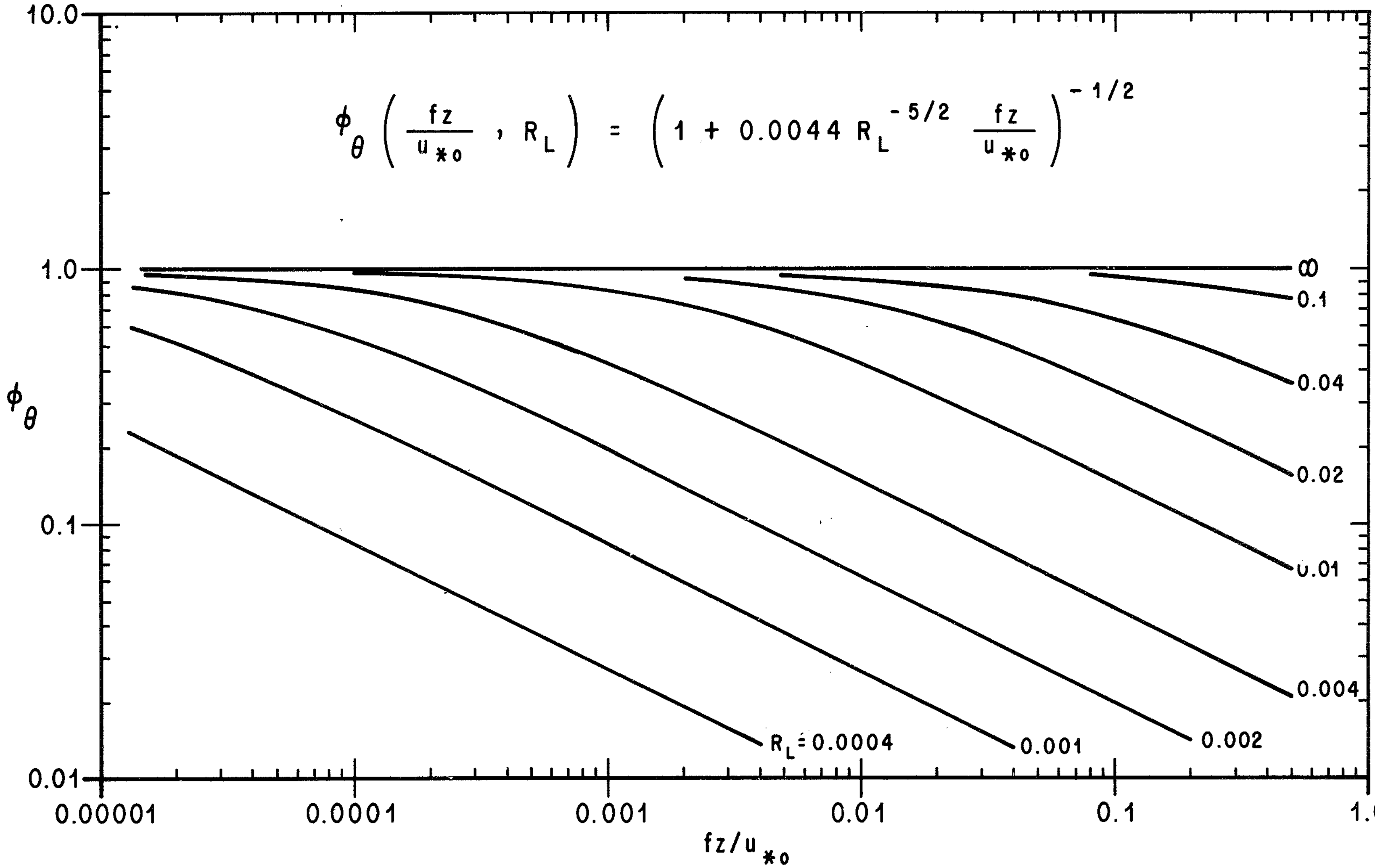

Figure 7. The Quantity ϕ_θ as a Function of fz/u_{*o} and R_L

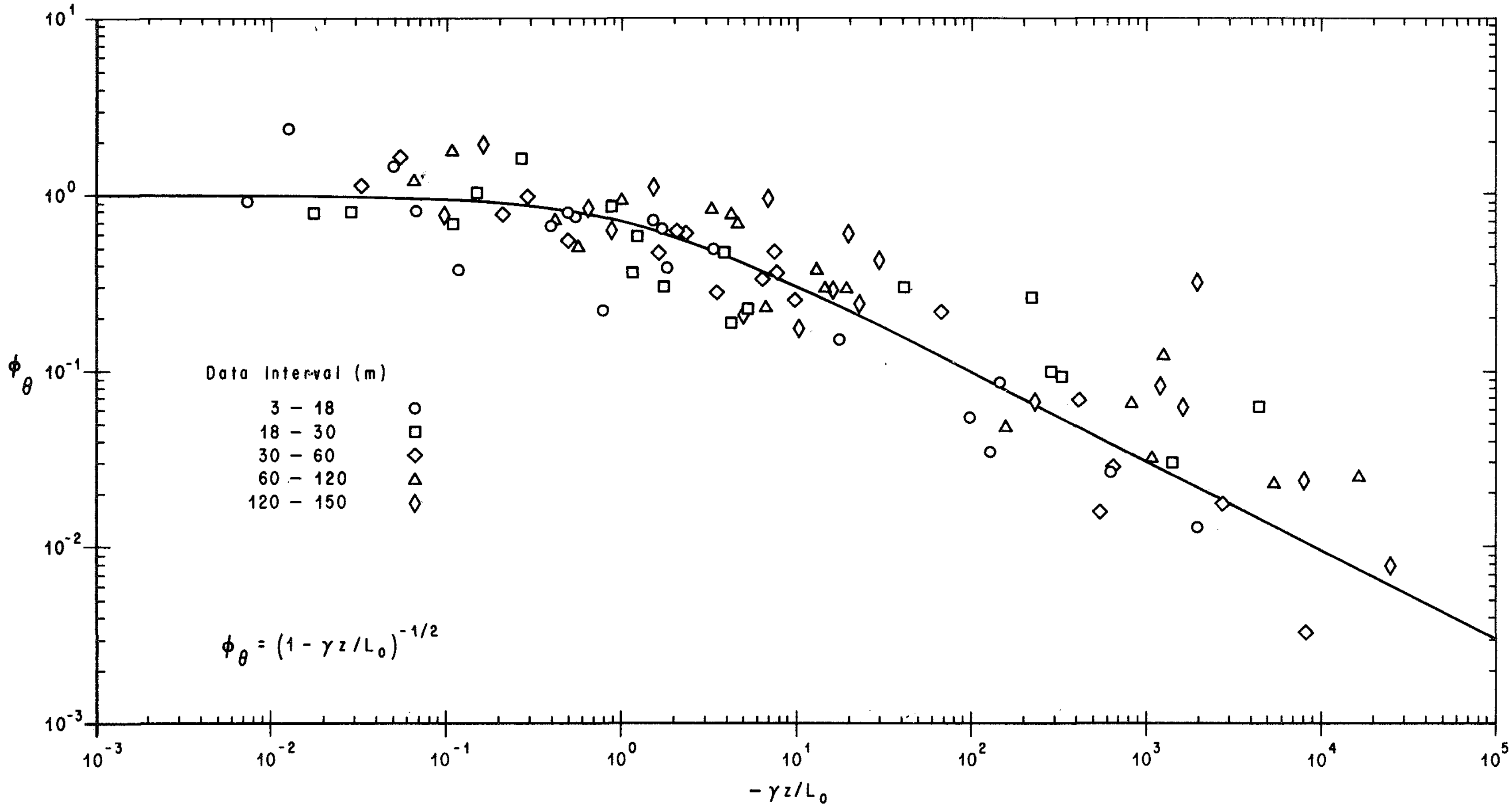

Figure 8. Experimental Values of ϕ_θ as a Function of $\gamma z/L_o$

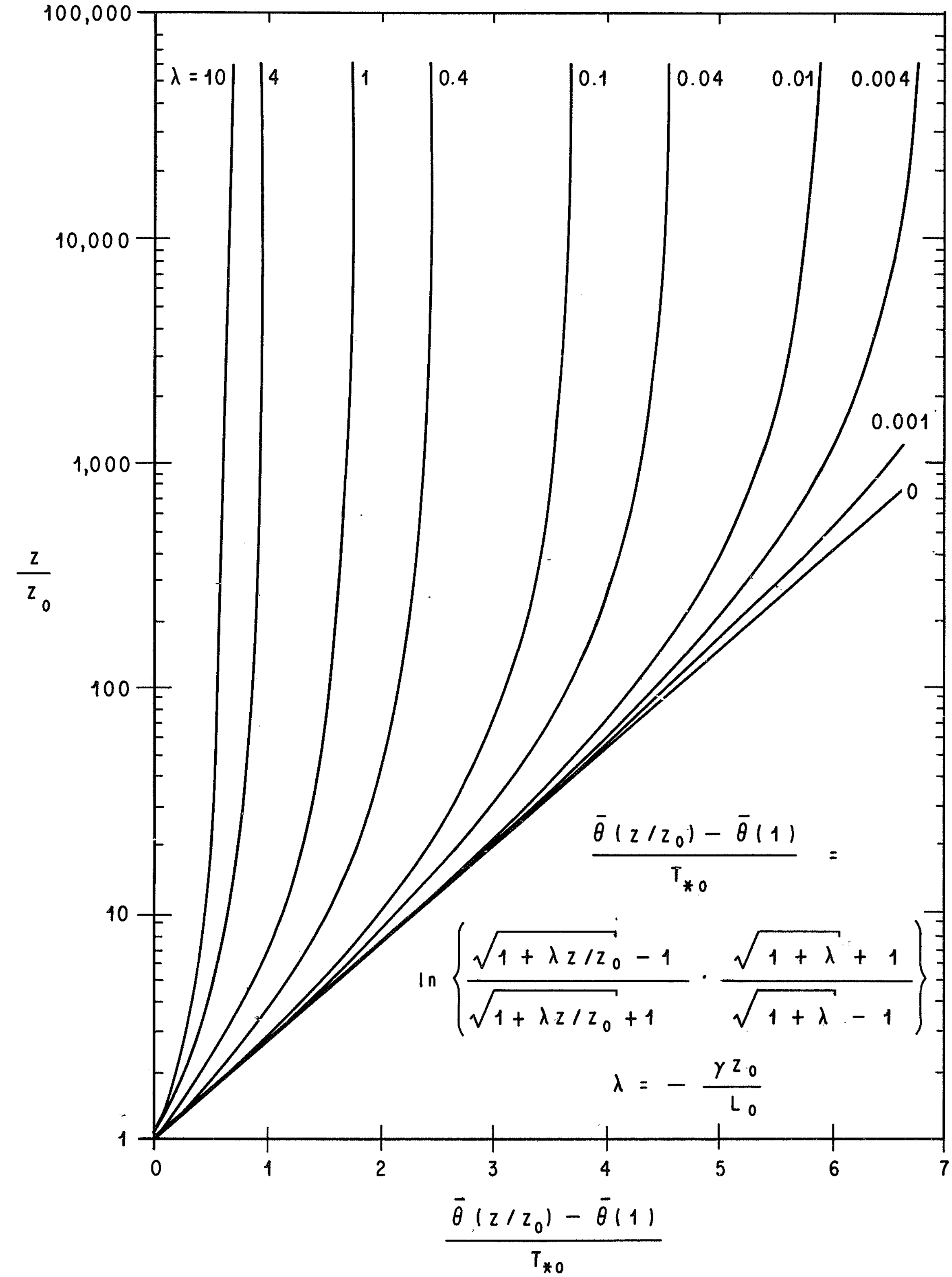

Figure 9. The Function $\Delta\bar{\theta}(z/z_o)/T_{*o}$ as a Function of z/z_o and λ

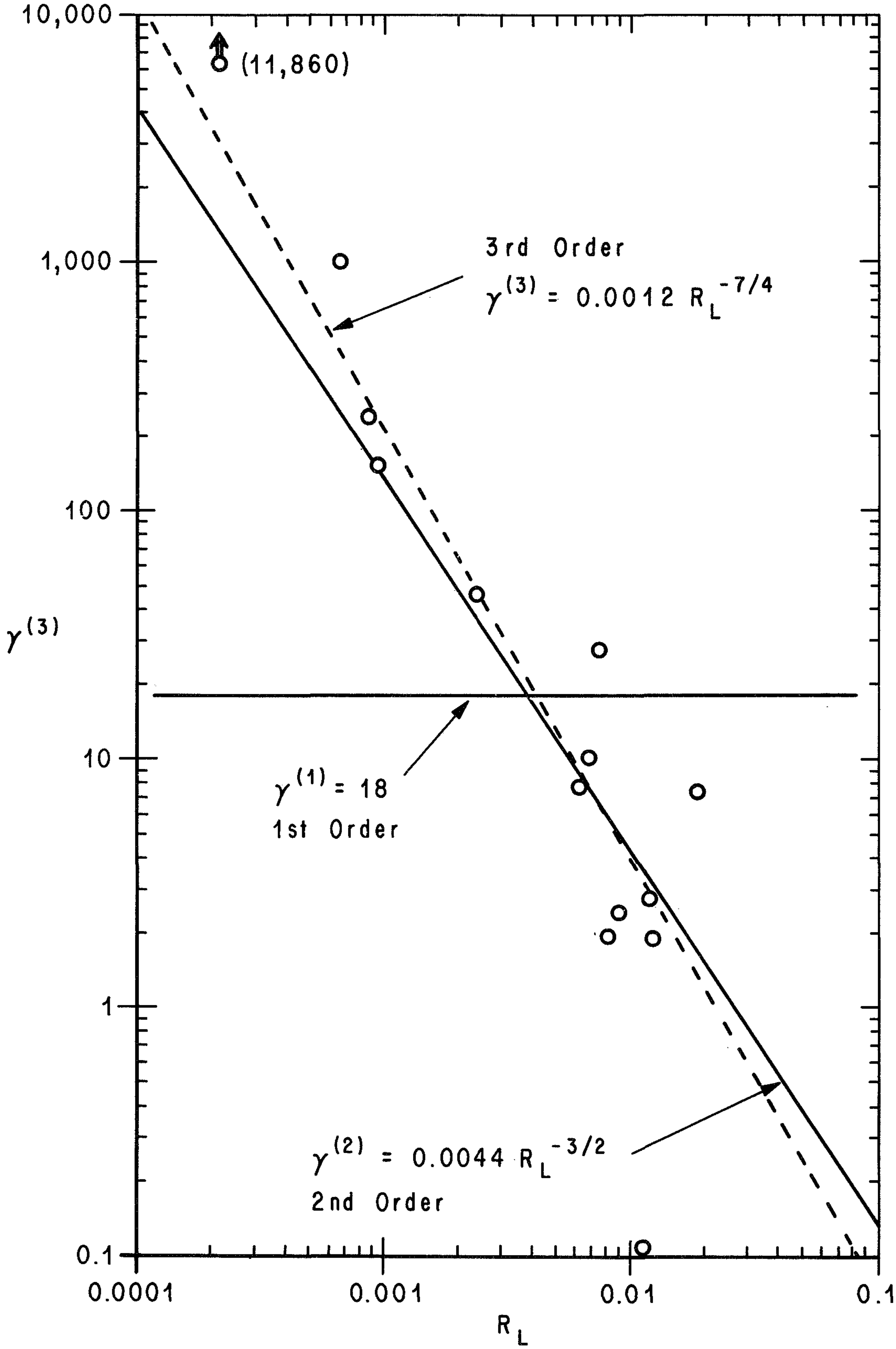

Figure 10. Third-Order Estimates of γ as a Function of R_L

APPENDIX A

Calculation of the Scaling Parameters u_{*o} and T_{*o}

In the unstable Monin layer, the dimensionless mean flow shear is a universal function of z/L_o, so that

$$\frac{k_1 z}{u_{*o}} \frac{\partial \bar{u}}{\partial z} = \phi_u(z/L_o), \tag{A-1}$$

where $\bar{u}(z)$ is the mean wind speed at height z, k_1 is von Karman's constant with numerical value approximately equal 0.4, u_{*o} is the surface friction velocity, and $\phi_u(z/L_o)$ is a universal function of z/L_o. The quantity L_o is the surface Monin-Obukhov stability length, namely,

$$L_o = - \frac{u_{*o}^3 \; C_p \bar{\rho} \; \bar{T}}{k_1 \; g \; H_o} . \tag{A-2}$$

In this equation H_o is the surface heat flux, $\bar{\rho}$ and $\bar{T}$ denote the mean flow density and Kelvin temperature, g is the acceleration of gravity, and C_p is the specific heat at constant pressure. The dimensionless shear ϕ_u is related to the flux Richardson number through the experimentally derived relationship

$$\phi_u = (1 - 18Ri)^{1/4}, \tag{A-3}$$

which is given in reference 6. The flux Richardson number is defined as

$$Ri = \frac{\frac{g}{\bar{\theta}} \frac{\partial \bar{\theta}}{\partial z}}{(\partial \bar{u}/\partial z)^2} , \tag{A-4}$$

where $\bar{\theta}$ is the mean potential temperature at height z. The flux Richardson number is a function of z/L_o. We shall invoke the Businger hypothesis [10] to relate Ri to z/L_o, so that

$$Ri = z/L_o. \tag{A-5}$$

Upon combining equations (A-1), (A-3), and (A-5) and integrating the resulting relationship, we find that

$$\bar{u}(z) = \frac{u_{*o}}{k_1}\left\{\ln\frac{z}{z_o} - \psi\left(\frac{z}{L_o}, \frac{z_o}{L_o}\right)\right\}, \tag{A-6}$$

where

$$\psi\left(\frac{z}{L_o}, \frac{z_o}{L_o}\right) = \int_{-z_o/L_o}^{-z/L_o} \frac{1 - (1 + 18\xi)^{-1/4}}{\xi}\, d\xi. \tag{A-7}$$

We have used the condition that $\bar{u}(z_o) = 0$ in the derivation of (A-6), where z_o is the surface roughness length. Equation (A-7) can be evaluated numerically for any value of z/L_o. The lower bound of this integral may be set equal to zero because the contribution to ψ from the region $0 < -z/L_o < -z_o/L_o$ is negligibly small. The surface friction temperature T_{*o} is defined as

$$T_{*o} = -\frac{1}{k_1 u_{*o}}\frac{H_o}{\bar{\rho}\, C_p}. \tag{A-8}$$

Equations (A-2) and (A-4) through (A-8) can be used to calculate the scaling velocity u_{*o}, the scaling temperature T_{*o}, and the surface Monin-Obukhov stability length. The procedure for calculating these quantities is as follows: (1) calculate the gradient Richardson number, equation (A-4), with the mean flow wind and potential temperature profile data in the Monin layer, (2) calculate L_o with equation (A-5), (3) calculate u_{*o} with (A-6) and (A-7), and (4) finally calculate T_{*o} with the results of steps (2) and (3) and (A-2) and (A-8).

The 18- and 30-meter temperature and wind data were used to estimate the Richardson number. The distributions of $\bar{u}(z)$ and $\bar{\theta}(z)$ between the 18- and 30-meter levels were assumed to be logarithmic profiles. The expressions for $\bar{u}(z)$ and $\bar{\theta}(z)$ were differentiated with respect to z and evaluated at the geometric height z = 23 meters to yield estimates of $\partial\bar{u}/\partial z$ and $\partial\bar{\theta}/\partial z$ for the calculation of Ri. This Richardson number was used to calculate L_o in step (2) above. The 18-meter level wind speed and $\psi(18\text{m}/L_o)$ were used to calculate u_{*o} in step (3).

The surface roughness lengths z_o that were associated with the NASA 150-meter meteorological tower site and that were used in the calculation of u_{*o} are given in reference 9.

APPENDIX B

Wind Speed and Temperature Profile Data and Other Parameters

The wind profile and temperature data that were used in this report are given in Tables B-1 and B-2. The 18-meter level wind direction is tabulated here because the surface roughness length at the NASA 150-meter tower facility is a function of wind direction. The values of Ri(23 m), L_o, u_{*o}, and T_{*o} that were calculated with these data are given in Table B-3.

TABLE B-1

Table of Temperature Profile Data*

(Temperature in °F)

Case No.	Date	Time (EST)	T(3m)	$(\Delta T)_1$	$(\Delta T)_2$	$(\Delta T)_3$	$(\Delta T)_4$	$(\Delta T)_5$
299	1/23/68	1315-1400	76.0	-1.41	-1.73	-2.56	-3.94	-4.58
305	1/26/68	1130-1230	52.4	-2.19	-2.66	-3.59	-5.01	-5.68
310	2/8/68	915-1015	40.5	- .32	-1.82	-2.86	-4.45	-5.09
319	2/26/68	1030-1130	59.0	-1.28	-2.63	-3.56	-5.01	-5.69
323	2/27/68	1200-1300	62.0	-1.80	-2.61	-3.57	-5.36	-5.95
332	3/1/68	1210-1310	49.0	-2.31	-2.94	-4.04	-5.73	-6.54
355	3/20/68	1330-1430	75.0	-1.82	-2.21	-2.99	-4.32	-4.99
359	3/22/68	1200-1300	77.0	-1.92	-2.97	-4.33	-5.57	-6.18
361	3/22/68	1320-1332	78.0	-2.00	-2.83	-4.17	-5.65	-6.01
364	3/27/68	1408-1438	73.0	-1.89	-2.32	-3.39	-4.86	-5.53
365	3/28/68	905-932	73.5	-1.44	-2.42	-3.12	-4.52	-5.26
366	3/28/68	1145-1245	74.5	-2.63	-3.13	-4.09	-5.62	-6.37
367	3/29/68	1010-1040	73.8	-1.45	-1.96	-2.61	-4.20	-5.18
406	4/7/68	1507-1537	79.0	-2.02	-2.57	-3.55	-4.88	-5.48
445	5/7/68	1400-1415	78.2	-2.29	-2.54	-3.74	-5.33	-5.99
515	6/16/68	1200-1300	83.0	-2.16	-2.60	-3.65	-5.31	-5.98
551	6/29/68	947-1027	79.8	- .93	-1.90	-2.48	-3.95	-4.52
554	6/30/68	933-952	83.1	-1.40	-1.91	-2.67	-4.04	-4.67
625	10/14/68	1100-1200	80.0	- .92	-1.91	-2.82	-4.51	-5.28

*$(\Delta T)_1$ = T(18m) - T(3m)

$(\Delta T)_2$ = T(30m) - T(3m)

$(\Delta T)_3$ = T(60m) - T(3m)

$(\Delta T)_4$ = T(120m) - T(3m)

$(\Delta T)_5$ = T(150m) - T(3m)

TABLE B-2

Table of Wind Speed and Direction Data

Case No.	18 m Wind Direction	$\bar{u}$(18 m) (m sec^{-1})	$\bar{u}$(30 m) (m sec^{-1})
299	219°	5.95	7.55
305	338°	8.50	9.31
310	298°	9.98	11.34
319	320°	4.81	5.13
323	317°	7.71	8.47
332	325°	7.20	7.79
355	83°	3.87	4.13
359	161°	5.29	5.69
361	161°	8.73	9.95
364	77°	6.08	6.40
365	95°	4.98	5.25
366	87°	6.12	6.48
367	115°	2.26	2.40
406	71°	4.36	4.73
445	93°	9.62	10.34
515	85°	5.96	6.38
551	34°	2.92	3.05
554	86°	4.01	4.12
625	38°	8.14	9.26

TABLE B-3

Table of Boundary Layer Parameters

Case No.	Ri(23 m)	L_o(m)	u_{*o}(m sec^{-1})	T_{*o} (°K)
299	-0.065	-357	0.52	-0.15
305	-0.090	-259	0.76	-0.41
310	-0.032	-716	1.20	-0.41
319	-2.448	- 9	0.48	-1.98
323	-0.234	- 99	0.61	-0.59
332	-0.276	- 84	0.58	-0.58
355	-0.557	- 42	0.36	-0.38
359	-1.148	- 20	0.56	-1.65
361	-0.089	-261	0.95	-0.66
364	-0.463	- 50	0.55	-0.80
365	-2.234	- 10	0.67	-3.54
366	-0.504	- 46	0.56	-0.88
367	-3.625	- 6	0.33	-1.22
406	-0.546	- 43	0.40	-0.48
445	-0.234	- 99	0.98	-1.52
515	-0.284	- 82	0.52	-0.50
551	-8.977	- 3	0.41	-3.62
554	-5.100	- 5	0.49	-3.58
625	-0.135	-172	0.69	-0.50

APPENDIX C

Correction of Finite Difference Estimates of Vertical Gradients of Potential Temperature

A first estimate of $\partial\bar{\theta}/\partial z$ can be obtained with finite differences, so that

$$(\partial\bar{\theta}/\partial z)^{(1)} = \frac{\bar{\theta}_2 - \bar{\theta}_1}{z_2 - z_1}, \tag{C-1}$$

where the superscript on $\partial\bar{\theta}/\partial z$ denotes the order of the estimate, and $\bar{\theta}_1$ and $\bar{\theta}_2$ are the potential temperatures at heights z_1 and z_2. A second and more precise estimate of $\partial\bar{\theta}/\partial z$ can be obtained by assuming that $\partial\bar{\theta}/\partial z$ is related to z through a power law

$$\partial\bar{\theta}/\partial z = az^q, \tag{C-2}$$

where a and q are constants. This assumption is appropriate if it is applied in a piecewise manner. The quantity q will vary between -1 and -2. Upon integrating (C-2) between levels z_1 and z_2, we find that

$$\bar{\theta}_2 - \bar{\theta}_1 = \frac{a}{1 + q}\left\{z_2^{1+q} - z_1^{1+q}\right\}. \tag{C-3}$$

Elimination of a between (C-2) and (C-3) and evaluation of the resulting relationship at the midpoint $z = (z_1 + z_2)/2$ of the interval $z_1 \leqq z \leqq z_2$ yield a second estimate of $\partial\bar{\theta}/\partial z$, so that

$$(\partial\theta/\partial z)^{(2)} = \frac{(1 + q)(\bar{\theta}_2 - \bar{\theta}_1)(z_2 + z_1)^q}{2^q\ (z_2^{1+q} - z_1^{1+q})}. \tag{C-4}$$

Upon forming the ratio between (C-1) and (C-4), we find

$$r = \frac{\phi_\theta^{(2)}}{\phi_\theta^{(1)}} = \frac{(1 + q)(1 - \xi)(1 + \xi)^q}{2^q(1 - \xi^{1+q})}, \tag{C-5}$$

where

$$\xi = z_2/z_1 \tag{C-6}$$

$$\phi_\theta^{(1)} = \frac{z_1 + z_2}{2T_{*o}} (\partial\bar{\theta}/\partial z)^{(1)} \tag{C-7}$$

$$\phi_\theta^{(2)} = \frac{z_1 + z_2}{2T_{*o}} (\partial\bar{\theta}/\partial z)^{(2)}. \tag{C-8}$$

Equations (C-1), (C-5), and (C-7) were used to estimate the dimensionless temperature gradient ϕ_θ. The procedure consisted of the following steps:

(1) Obtain a first estimate of $\partial\bar{\theta}/\partial z$ with (C-1).

(2) Calculate a first estimate of the dimensionless potential temperature gradient $\phi_\theta^{(1)}$ at $z = (z_1 + z_2)/2$ with (C-7),

(3) Plot $\phi_\theta^{(1)}$ as a function of $-z/L_o$ on bilogarithmic graph paper and estimate piecewise values of q.

(4) Calculate the quantity r with (C-5) using the results of (3).

(5) Calculate a second estimate of ϕ_θ by multiplying the values of $\phi_\theta^{(1)}$ obtained in step (2) with r.

The results of step (5) above were used to model the potential temperature profile.

A plot of r as a function of q for ξ = 0.167, 0.5, 0.6, and 0.8 is shown in Figure C-1. These values of r correspond to the ratios between heights appropriate for the NASA 150-meter meteorological tower site.

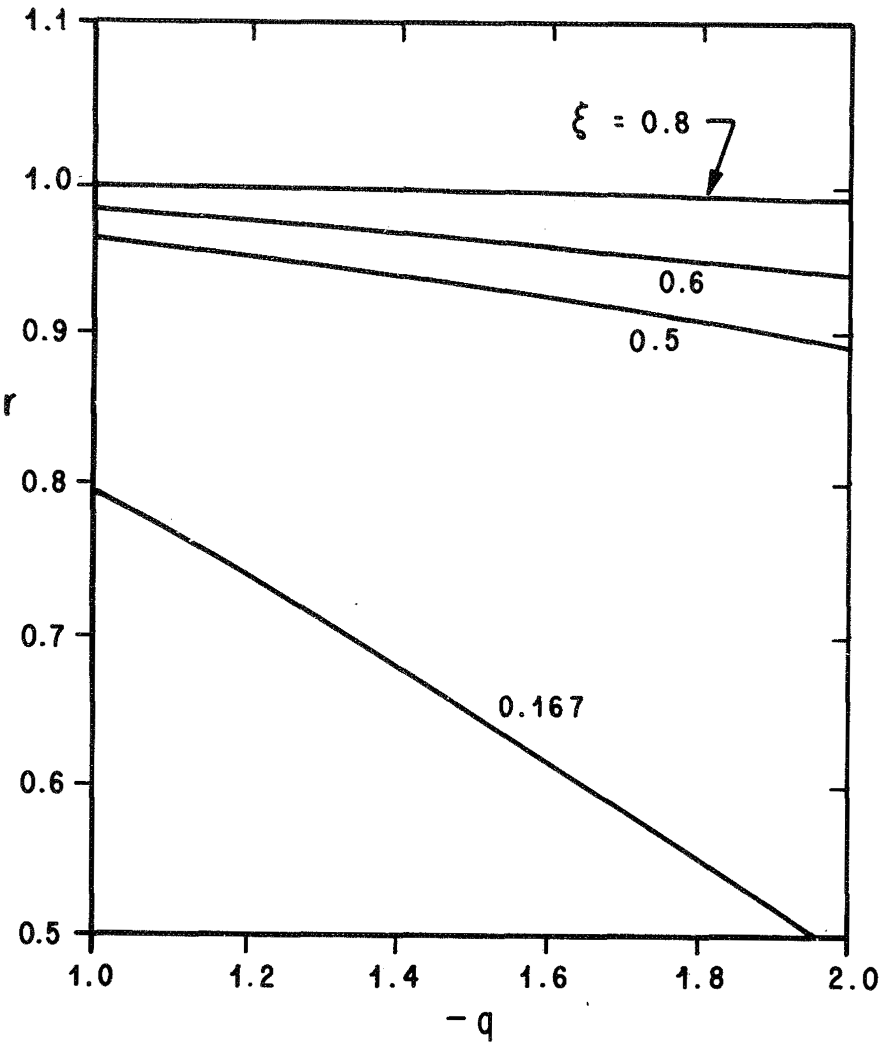

Figure C-1. The Quantity r as a Function of q for Various Values of ξ

REFERENCES

1. Dyer, A. J., "The Turbulent Transport of Heat and Water Vapor in an Unstable Atmosphere," Quart. J. R. Meteor. Soc., 93, 501-508, 1967.

2. Pandolfo, J. P., "Wind and Temperature Profiles for Constant-Flux Boundary Layers in Lapse Conditions with a Variable Eddy Conductivity to Eddy Viscosity Ratio," J. Atmos. Sci., 23, 495-502, 1966.

3. Prasad, B. and H. A. Panofsky, "Properties of Variances of the Meteorological Variables at Round Hill," Final Report RCS-OSD-1366, The Pennsylvania State University, pp. 65-95, 1967.

4. Blackadar, A. K. and H. Tennekes, "Asymptotic Similarity in Neutral Barotropic Planetary Boundary Layers," J. Atmos. Sci., 25, 1015-1020, 1968.

5. Blackadar, A. K., "Wind Velocity Profiles," Ann. N. Y. Acad. Sci., Vol. 116(1), 101-115, 1964.

6. Lumley, J. L. and H. A. Panofsky, The Structure of Atmospheric Turbulence, Interscience Publishers, John Wiley & Sons, New York, 239 pp., 1964.

7. Langhaar, H. L., Dimensional Analysis and Theory of Models," John Wiley and Sons, New York, 166 pp., 1951.

8. Kaufman, J. W. and L. F. Keene, "NASA's 150-meter Meteorological Tower Located at the Kennedy Space Center, Florida," NASA TM X-53699, 1968.

9. Fichtl, G. H. and G. E. McVehil, "Longitudinal and Lateral Spectra of Turbulence in the Atmospheric Boundary Layer at the Kennedy Space Center," J. Appl. Meteor, 9, 51-63, 1970.

10. Panofsky, H. A., "Spectra of the Horizontal Wind Components," NASA Contractor Report NASA CR-1410, 69-83, 1969.

11. Blackadar, A. K. and J. K. S. Ching, "Wind Distribution in a Steady-State Planetary Boundary Layer of the Atmosphere with Upward Turbulent Heat Flux," Final Report, Contract No. AF(604)-6641, pp. 23-48, 1965.

APPROVAL NASA TM X-64519

THE POTENTIAL TEMPERATURE PROFILE IN THE PLANETARY BOUNDARY LAYER

by George H. Fichtl and Julian F. Nelson

The information in this report has been reviewed for security classification. Review of any information concerning Department of Defense or Atomic Energy Commission programs has been made by the MSFC Security Classification Officer. This report, in its entirety, has been determined to be unclassified.

This document has also been reviewed and approved for technical accuracy.

W. W. Vaughan
Chief, Aerospace Environment Division

E. D. Geissler
Director, Aero-Astrodynamics Laboratory